U.S. DEPARTMENT OF ENERGY | Office of Science

DOE/SC-ARM-25-003

Examining the Ice-Nucleating Particles from the North Slope of Alaska (ExINP-NSA) Final Campaign Report

N Hiranuma
O Talukder
AD Pantoya

April 2025

ARM

DISCLAIMER

DOE/SC-ARM-25-003

Examining the Ice-Nucleating Particles from the North Slope of Alaska (ExINP-NSA) Final Campaign Report

N Hiranuma, West Texas A&M University
Principal Investigator

AD Pantoya, West Texas A&M University
O Talukder, West Texas A&M University
Co-Investigators

April 2025

Work supported by the U.S. Department of Energy,
Office of Science, Office of Biological and Environmental Research

Acronyms and Abbreviations

ARM	Atmospheric Radiation Measurement
BRW	Barrow Atmospheric Baseline Observatory
DOE	U.S. Department of Energy
ENA	Eastern North Atlantic
ExINP-NSA	Examining the Ice-Nucleating Particles from the North Slope of Alaska
HPLC	High-performance liquid chromatography
INP	Ice-nucleating particle
LPM	Liter per minute
nINP	Number concentration of ice-nucleating particle
ns	nINP scaled to total surface area concentration of aerosols
NOAA	National Oceanographic and Atmospheric Association
NSA	North Slope of Alaska
OPS	Optical particle sizer
PINE-03	Portable ice nucleation experiment version 3
Saer	Total surface area concentration of aerosols
SGP	Southern Great Plains
UTC	Coordinated Universal Time
WD	Wind direction
WT-CRAFT	West Texas cryogenic refrigerator applied to freezing test

Contents

Figures

Tables

1.0 Summary

The Examining the Ice-Nucleating Particles from the North Slope of Alaska (ExINP-NSA) campaign was conducted at the National Oceanic and Atmospheric Administration's (NOAA) Barrow Atmospheric Baseline Observatory (71.3230° N, 156.6114° W, "BRW" hereafter), next to the Atmospheric Radiation Measurement (ARM) user facility NSA site and ~ 6 km northeast of the town of Utqiaġvik. The location of the NSA site is shown in Figure 1. Our observing period began in October 2021 and continued until May 2024.

This campaign was funded by the U.S. Department of Energy (DOE) Office of Science Early Career Research Program through grant number DE-SC001879. This grant contains funding for three ARM field campaigns. The previous field campaigns were performed at ARM's Southern Great Plains atmospheric observatory in Oklahoma (SGP; 36.6073° N, 97.4876° W) and the ARM's Eastern North Atlantic atmospheric observatory on Graciosa Island, Azores (ENA; 39.0916° N, 28.0257° W). The ExINP-NSA campaign aims included:

- Determining the number concentration of ice-nucleating particles (n_{INPs}) active at temperatures spanning the range of heterogeneous freezing processes (from ≈−30 °C to 0 °C) using a combination of online and offline measurements
- Determining whether local meteorological conditions and/or synoptic scale air mass transport impact INP abundance and/or ice nucleation efficiency
- Examining if the physicochemical properties of INPs relate to aerosol chemistry
- Assessing if there is a similarity in INP properties across three ARM sites

Multi-seasonal datasets of INP abundance in the NSA region were delivered from this campaign. This campaign also allowed researchers to perform a comprehensive analysis of atmospheric INPs based on long-term ground-based measurements in the Alaskan Arctic. Our data and results from the ExINP-NSA campaign will help refine current earth system models. One of the stated goals of ARM is to advance aerosol-cloud ice interaction, which will be a direct result of this campaign. Current earth system models poorly represent INPs, and the 15-minute time resolution data over several seasons generated during this campaign will provide an invaluable resource, especially combined with the datasets generated during two previous ARM ExINP campaigns. These datasets will allow for a greater understanding of ice nucleation processes as they may (or may not) relate to local meteorological processes and aerosol chemistry and will eventually help further the understanding of the Earth's atmospheric processes and energy balance.

We utilized a portable ice nucleation experiment chamber ver. 3 (PINE-03) to collect high-resolution data over a nearly 32-month period and analyze aerosol and meteorological data to assess the correlation between ambient n_{INP}, air mass origin region, and meteorological variability. The PINE-03 system measures ambient n_{INP} *in situ* using a simulated adiabatic expansion cooling method (Möhler et al., 2021). This system is a commercialized product, resulting in consistent operation amongst studies (Möhler et al., 2021; Knopf et al., 2021; Lacher et al., 2024; Wilbourn et al., 2024) compared to traditional INP monitoring devices that are typically custom-built by individual scientists. Besides relatively high measurement time resolution (≲ 12 min), the advantages of PINE-03 include (1) no substantial artifacts (e.g., no ice off of the vessel

wall); (2) remote operation capability with minimum in-person maintenance or supervision requirements; and (3) fast turnover time to scan freezing temperatures in a wide range (Wilbourn et al., 2024).

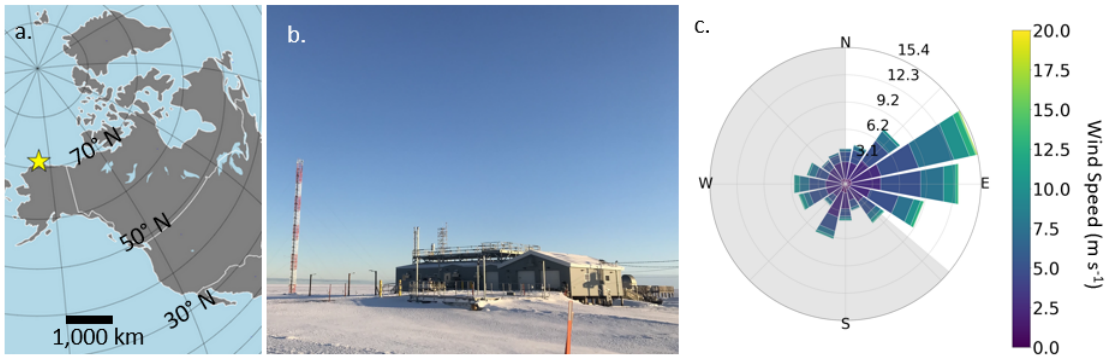

Figure 1. The location of the ExINP-NSA campaign on the NSA site is indicated with a yellow star on the map (a). The photo of the observatory is shown in picture (b). The wind speed and direction distributions during the ExINP-NSA (October 2021 − December 2023) are shown in the wind rose plot (c). The grey shaded area represents the flagged wind direction (130° < WD < 360°), indicating potential contamination from Utqiaġvik.

Figure 2 shows an experimental schematic of the ExINP-NSA campaign. At the beginning of the campaign, we measured the loss of particles in the inlet used at the BRW site (presumably due to gravitational settling and diffusion loss) using an optical particle sizer, OPS (model 3330, TSI Inc.) (Figure 2b). Briefly, we moved an OPS back and forth between the downstream position of the inlet inside the BRW site and the roof of the building to examine the difference in particle size distributions in ambient air vs. air through the inlet and characterize the associated particle loss through the inlet. The inlet was composed of a polyvinyl chloride stack and stainless steel sampling pickup inlets (3/4 inch outer diameter) connected to a vertical sampling stack (4-inch diameter, 12 m height above ground level). A 3/8-inch conductive tube bridged the pickup port to the suite of instruments in the observatory. The total flow down the polyvinyl chloride stack was set to ≈ 260 Liters Per Minute (LPM) during the entire study period, and we sub-sampled from the center of the stack. As shown in Figure 2c, the aerosol particle diameters corresponding to the 50% particle loss through the stack inlet from the ExINP-NSA campaign was 2.3 µm in optical diameter. This size is slightly smaller than the 50% particle loss of the PINE-03 chamber (i.e., 4 µm in aerodynamic diameter) under the spherical assumption. Thus, our INP measurement was limited to this particle loss size.

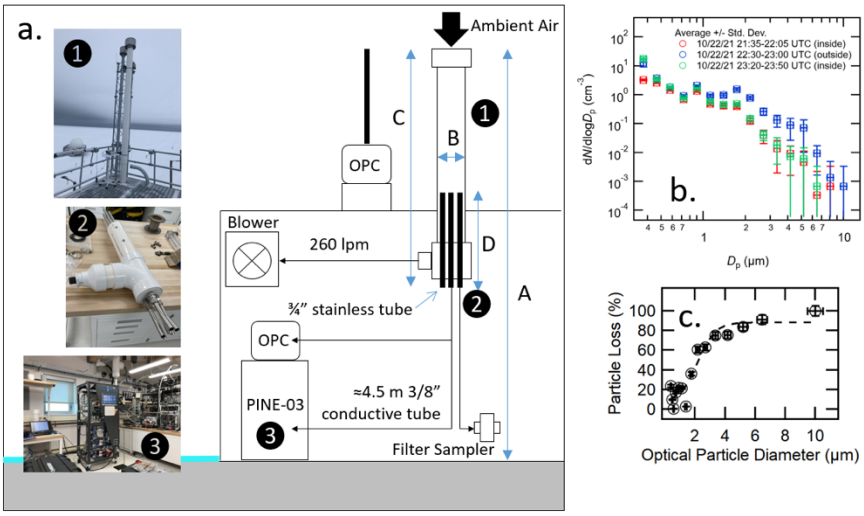

Figure 2. Panel (a) shows an experimental schematic of the particle loss test through the PVC stack inlet at the BRW site (A = 12 m; B = 0.1 m; C = 7.6 m; D = 0.9 m). Panels (b) and (c) show the particle size distributions measured inside and outside the observatory and particle loss through the inlet as a function of particle diameter. Each data point is shown ± a 5% size uncertainty on the x-axis and ± the standard deviation of three measurements on the y-axis (20-second time average for each data point). The filter sampler was used for collecting particles for offline INP analysis. This figure is adopted from Pantoya et al. (submitted).

To complement the PINE-03 data for relatively high freezing temperatures (> −15 °C), we collected filter samples that were later analyzed using an offline freezing assay called West Texas Cryogenic Refrigerator Applied to Freezing Test (WT-CRAFT). This technique has been applied to INP abundance measurements of samples from another arctic site, Ny-Ålesund (Li et al., 2023; Rinaldi et al., 2021). Particle samples were collected onto polycarbonate Whatman Nuclepore 47 mm filters (0.2 µm diameter pore size) in the selected period (see Supplementary Table S1), typically for a day to three days. Sampled air volume was estimated based on the sampling airflow and period for each filter. Filters were then stored in sterile Petri dishes at −20 °C (other than during transportation between BRW and Texas, when they were stored at ambient temperatures) prior to analysis, which occurred no more than one year after collection. Filters were washed in high-performance liquid chromatography (HPLC)-grade water (Sigma Aldrich) to suspend particle samples. The ice nucleation ability of these aerosols was then tested by plating on a machined aluminum plate inside a cryocooler that cooled the sample at a rate of 1 °C per minute. We assessed freezing temperatures between 0 °C and −25 °C, which is reasonable for this study as they are relevant to arctic mixed-phase clouds (e.g., Shupe, 2011; de Boer et al., 2011). Based on the number of droplets frozen, the n_{INP} value was calculated using an equation based on calculations given in Vali (1971). Samples collected on filters were also treated with 100 °C heat to remove heat-sensitive material, including but not limited to proteins, which denature at temperatures above approximately 60 °C (Hogg, 2013). A 1 mL portion of the suspension containing the sample was placed into a sterile 15 mL polycarbonate tube (VWR), which was then capped and placed into a beaker of boiling water for 20 min. The sample was allowed to cool, then n_{INP} was measured with WT-CRAFT. The heat-treated sample was also diluted as needed to collect data down to −25 °C.

2.0 Results

Continuous n_{INP} data were collected in the Alaskan Arctic from October 2021 through May 2024. Shown in Figure 3 is the comparison of online $n_{INP}(T)$ based on (a) the 'all' dataset (i.e., all valid measurements retained), (b) 'clean' data subset as determined following the standard BRW wind protocols and removing flagged PINE-03 data for operational issues; and (c) 'contaminated' subset following the wind and PINE-03 data screening protocols (Pantoya et al., submitted). The time series of 6 h averaged $n_{INP}(T)$ from BRW with a temperature resolution of 1 °C is shown in each panel, with different colors scaling to the freezing temperature between −16 °C (red) and −31 °C (blue). For the 'all' dataset, the $n_{INP}(T)$ data are displayed with a total of 19,835 data points of 6 h averaged $n_{INP}(T)$ collected during our study period. The data gaps in several seasons seen in Figure 3 are due to maintenance, as required every few months.

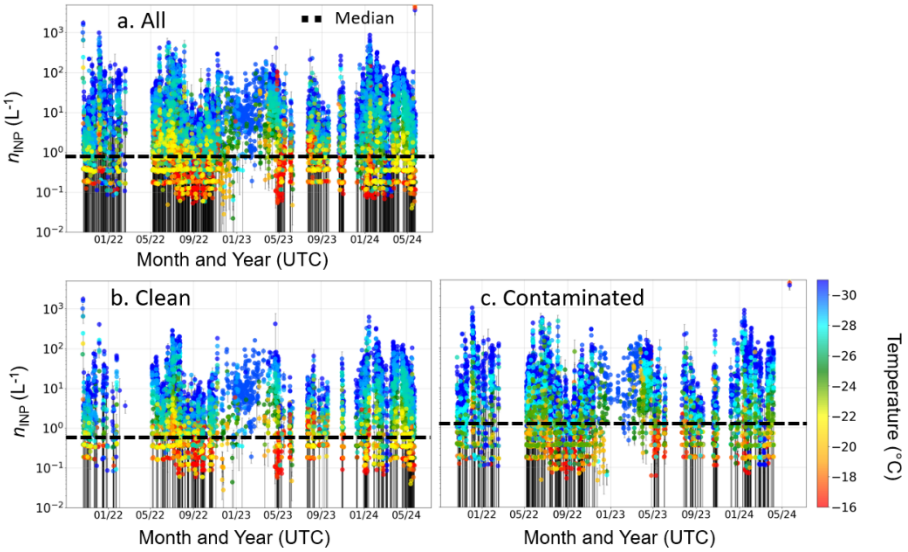

Figure 3. $n_{INP}(T)$ measured at BRW. The 'all' dataset collected throughout the campaign is shown in (a). The segregated datasets collected during the 'clean' periods and 'contaminated' periods are shown in (b) and (c). Each data is 6-hour time-averaged. The color scale indicates the measured freezing temperature. Individual data points are temperature binned for 1 °C. The vertical error bars represent the standard error of time-averaged data. The campaign mean and median $n_{INP}(-25°C)$ are shown with dark blue and cyan lines.

For freezing temperatures from −16 to −31 °C, clean $n_{INP}(T)$ data show the lowest median. The distribution of $n_{INP}(T)$ is skewed due to the occurrence of positive extremes. Thus, we report the median. As shown in Figure 3, $n_{INP}(-25°C)$ median values ± standard errors are 0.8 ± 0.4 L^{-1}, 0.7 ± 0.2 L^{-1}, and 1.1 ± 0.4 L^{-1} for all clean and contaminated datasets, respectively. Likewise, the medians of $n_{INP}(-25°C)$ are similarly sorted with 0.8 ± 0.4 L^{-1}, 0.6 ± 0.2 L^{-1}, and 1.1 ± 0.5 L^{-1} for all, clean, and contaminated datasets. The contaminated dataset exhibited a higher value than the others, likely due to the emissions from Utqiaġvik.

Freezing efficiency of BRW INPs, $n_s(T)$, was computed based on PINE-03 and WT-CRAFT data (Figs. 4 and 5, respectively) by scaling $n_{INP}(T,t)$ to the total surface area concentration of aerosols at the given time ($S_{aer}(t)$) according to the data provided in Pantoya et al. (submitted). Figure 4a shows 6-hour averaged PINE-03-measured n_{INP} and n_s data from BRW as a function of freezing temperatures (for October 2021 to December 2023) as box plots (a − b). Clean data were used to generate Figure 4 and did not include

any identified artifacts. Also shown in Figure 4 are previously reported $n_{INP}(T)$ data collected from or near the North Slope of Alaska (see Pantoya et al. and references therein). The data collected in this study are generally comparable to data presented in previous studies as their data overlap with our 25th – 75th percentile $n_{INP}(T)$ data in one temperature bin at least. On the other hand, the $n_{INP}(T)$ range for some studies is much lower than the $n_{INP}(T)$ range of ExINP-NSA, potentially due to differences in INP sources that those studies investigated (e.g., sea spray aerosols without sea ice coverage). As seen in Figure 4b, we find a factor of 10 − 1000 times greater efficiency in the arctic INPs from BRW than those found previously at the mid-latitude ARM sites by PINE-03. Relatively low concentrations of aerosol surface area and contrasting high INP concentrations at BRW relative to mid-latitude sites might explain it. Following Li et al. (2022) and Wilbourn et al. (2024), we computed $n_s(T)$ parameterizations that fit the average values of the log-normal $n_s(T)$ distribution as a function of freezing temperatures as follows (r = 0.99):

$$n_s^{avg}(T) = exp\left(24.250 \times exp\left(-exp\left(0.060 \times (T + 9.700)\right)\right) + 4.995\right) \quad -31\,°C \le T \le -21\,°C \quad [1].$$

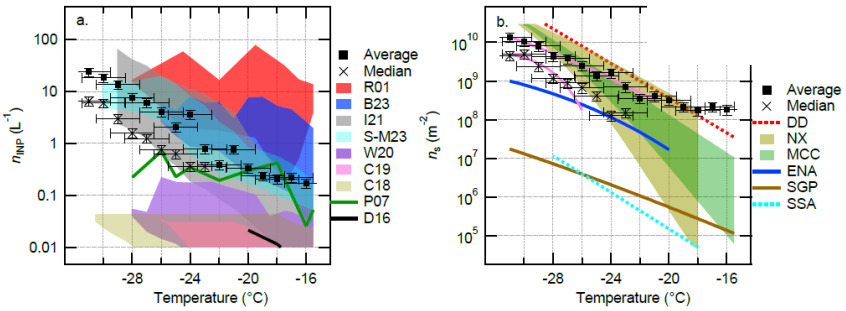

Figure 4. $n_{INP}(T)$ (a) and $n_s(T)$ (b) data are adopted from Pantoya et al. (submitted). The 'clean' data were used to generate this figure. Boxes represent average (black solid symbol) and median (black open symbol) statistics. The color-shaded area in (a) shows the maximum and minimum $n_{INP}(T)$ measured by previous INP studies at or in the proximity of BRW (see Pantoya et al). The reference $n_s(T)$ data in (b) are adopted from W24 (Wilbourn et al., 2024 and references therein). Pink lines are fits to BRW data from this study.

To generate the data presented in Figure 5, polycarbonate filters were taken at BRW during several focus fieldwork periods over multiple meteorological seasons (October 22 to December 20, 2021, June 6 to June 27, 2022, and August 29 to October 28, 2022, all in UTC) for ambient samples (Figure 5a) and heat-treated samples (Figure 5b). A summary of the ambient aerosol particle filter sampling conditions at BRW is available in Table S1. For our study periods, median n_s values from filters range from 3.3 x 10^7 m^{-2} (heated) to 1.4 x 10^8 m^{-2} (unheated) at −25 °C, which represents the lowest temperature measured with WT-CRAFT. Overall, the minimum-maximum $n_s(T)$ values range from 1.3 x 10^5 m^{-2} (−5.5 °C) to 1.5 x 10^{10} m^{-2} (−25 °C), with the concentration generally increasing with decreasing temperature. The $n_s(T)$ values measured from filter samples decreased with heat treatment for 30.2 – 100% at −20 °C. The average suppression in n_s(−20 °C) after heat treatment was 79.6%. A reduction in INPs can be attributed to heat-labile aerosols.

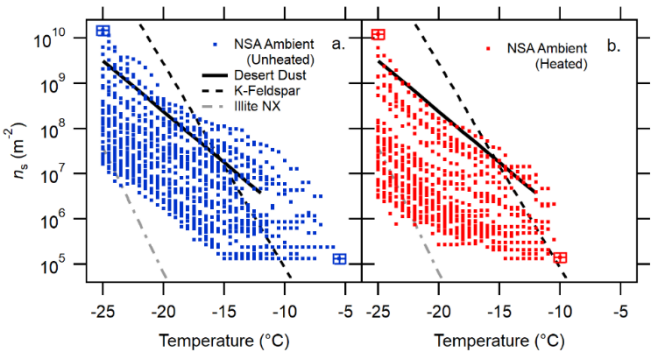

Figure 5. A summary of $n_s(T)$ data at each 0.5°C temperature interval for both (a) untreated and (b) heated ambient particle samples from BRW is shown. The reference $n_s(T)$ spectra in panels (a) and (b) are for previously characterized INPs, such as desert dust (≤−12 °C; Niemand et al., 2012), illite NX (≤−11 °C; Hiranuma et al., 2015), and K-feldspar (< −5 °C; Atkinson et al., 2013). Error bars shown only for the first and last data points for each panel (to retain the data visibiity) represent ± 0.5 °C temperature uncertainties on the x-axis (systematic error) and ±23.5% on the y-axis (statistical error) according to Hiranuma et al. (2019).

To illuminate patterns in $n_s(T)$, the PINE-03 chamber data were compared with several different measurements made by collocated instruments maintained as part of the ongoing measurements being made at BRW. From back trajectory analysis, air masses observed during high INP episodes in spring tended to come from local terrestrial regions (Pantoya et al., submitted). The presence of low pressure over the Aleutian Islands may trigger the synoptic-scale transport of warm North Pacific air to northern Alaska, delivering air masses containing freezing active INPs, such as local dust and marine biogenic compounds (Cox et al., 2019; Inoue et al., 2021).

The difference between offline and online was expected for the reasons discussed in Wilbourn et al. (2024), summarizing our previous ARM field observation study. The observed discrepancy is not an area of concern or focus for this campaign report. There may be several factors driving this discrepancy in $n_s(T)$, including (but not limited to) the difference in sampling time intervals, measured freezing processes, and potential decay of freezing ability of presumably biogenic particles collected on filters that were stored at −20 °C until processing. These factors may result in a potential for higher $n_{INP}(T)$ in PINE-03 when compared with $n_{INP}(T)$ measured at the same temperature from samples collected on filters.

The Outlook of this project includes the publication of a paper regarding PINE-03, other aerosol physicochemical properties, and meteorological data from BRW (submitted to Aerosol Research), as well as the publication of a paper contextualizing local and synoptic meteorological influences on INPs. Future work in NSA may target to improve atmospheric models to simulate cloud feedback and determine their impact on the global radiative energy budget and additional aerosol data, such as size-resolved particle chemical composition and mixing state. These extra measurements would allow us to understand further the implications of this dataset for clouds, precipitation, and regional weather, as well as overall ambient ice nucleation propensity in the NSA region. Vertical INP profiling, as well as INP measurements in snow samples, will be useful for further understanding of the arctic INP transport and source. Aerosol-aware INP parameterization (e.g., Burrows et al., 2022) and comparison of predicted vs. observed n_{INP} in the Arctic must be investigated.

3.0 Publications and References

Publication

Pantoya, AD, and N Hiranuma.2024. The abundance of ground-level atmospheric ice-nucleating particles and aerosol properties in the North Slope of Alaska. figshare. Dataset, Ffgshare, https://doi.org/10.6084/m9.figshare.26615752.v3

Pantoya, AD, SR Simonsen, E Andrews, R Burgener, CJ Cox, G de Boer, BD Thomas, and N Hiranuma. 2025. "Multi-seasonal measurements of the ground-level atmospheric ice-nucleating particle abundance on the North Slope of Alaska." Aerosol Research Discussion [preprint], https://doi.org/10.5194/ar-2025-1, submitted

References

Atkinson, JD, BJ Murray, MT Woodhouse, TF Whale, KJ Baustian, KS Carslaw, S Dobbie, D O'Sullivan, and TL Malkin. 2013. "The importance of feldspar for ice nucleation by mineral dust in mixed-phase clouds." *Nature* 498, 355–358, doi:10.1038/nature12278

Burrows, SM, CS McCluskey, G Cornwell, I Steinke, K Zhang, B Zhao, M Zawadowicz, A Raman, G Kulkarni, and S China. 2022. "Ice-nucleating particles that impact clouds and climate: observational and modeling research needs." *Reviews of Geophysics* 60, e2021RG000745, https://doi.org/10.1029/2021RG000745

Cox, CJ, RS Stone, DC Douglas, DM Stanitski, and MR Gallagher. 2019. "The Aleutian Low-Beaufort Sea Anticyclone: A climate index correlated with the timing of springtime melt in the Pacific Arctic cryosphere." *Geophysical Research Letters* 46, 7464–7473, https://doi.org/10.1029/2019GL083306

de Boer, G, H Morrison, H, MD Shupe, and R Hildner. 2011. "Evidence of liquid dependent ice nucleation in high-latitude stratiform clouds from surface remote sensors." *Geophysical Research Letters* 38, L01803, https://doi.org/10.1029/2010GL046016

Hiranuma, N, K Adachi, DM Bell, F Belosi, H Beydoun, B Bhaduri, H Bingemer, C Budke, H-C Clemen, F Conen, KM Cory, J Curtius, PJ DeMott, O Eppers, S Grawe, S Hartmann, N Hoffmann, K Höhler, E Jantsch, A Kiselev, T Koop, G Kulkarni, A Mayer, M Murakami, BJ Murray, A Nicosia, MD Petters, M Piazza, M Polen, N Reicher, Y Rudich, A Saito, G Santachiara, T Schiebel, GP Schill, J Schneider, L Segev, E Stopelli, RC Sullivan, K Suski, M Szakáll, T Tajiri, H Taylor, Y Tobo, R Ullrich, D Weber, H Wex, TF Whale, CL Whiteside, K Yamashita, A Zelenyuk, and O Möhler. "A comprehensive characterization of ice nucleation by three different types of cellulose particles immersed in water." *Atmospheric Chemistry Physics* 19, 4823–4849, https://doi.org/10.5194/acp-19-4823-2019

Hogg, S. 2013. Essential microbiology, John Wiley & Sons, New York, NY, USA, 528 pp., ISBN 978-1-119-97890-9

Inoue, J, Y Tobo, F Taketani, and K Sato. 2021. "Oceanic supply of ice-nucleating particles and its effect on ice cloud formation: A case study in the Arctic ocean during a cold-air outbreak in early winter." *Geophysical Research Letters* 48, e2021GL094646, https://doi.org/10.1029/2021GL094646

Knopf, DA, KR Barry, TA Brubaker, LG Jahl, KA Jankowski, J Li, Y Lu, LW Monroe, KA Moore, FA Rivera-Adorno, KA Sauceda, Y Shi, JM Tomlin, HSK Vepuri, P Wang, NN Lata, EJT Levin, JM Creamean, TCJ Hill, S China, PA Alpert, RC Moffet, N Hiranuma, RC Sullivan, AM Fridlind, M West, N Riemer, A Laskin, PJ DeMott, and X Liu. 2021. "Aerosol-ice formation closure: A Southern Great Plains field campaign.", Bulletin of the American Meteorological Society 102, E1952–E1971, https://doi.org/10.1175/Bams-D-20-0151.1

Lacher, L, MP Adams, K Barry, B Bertozzi, H Bingemer, C Boffo, Y Bras, N Büttner, D Castarede, DJ Cziczo, PJ DeMott, R Fösig, M Goodell, K, Höhler, TCJ Hill, C Jentzsch, LA Ladino, EJT Levin, S Mertes, O Möhler, KA Moore, BJ Murray, J Nadolny, T Pfeuffer, D Picard, C Ramírez-Romero, M Ribeiro, S Richter, J Schrod, K Sellegri, F Stratmann, BE Swanson, ES Thomson, H Wex, MJ Wolf, and E Freney. 2024. "The Puy de Dôme ICe Nucleation Intercomparison Campaign (PICNIC): comparison between online and offline methods in ambient air." *Atmospheric Chemistry Physics* 24, 2651–2678, https://doi.org/10.5194/acp-24-2651-2024

Li, G, EK Wilbourn, Z Cheng, J Wieder, A Fagerson, J Henneberger, G Motos, R Traversi, SD Brooks, M Mazzola, S China, A Nenes, U Lohmann, N Hiranuma, ZA and Kanji. 2019. "Physicochemical characterization and source apportionment of Arctic ice-nucleating particles observed in Ny-Ålesund in autumn." *Atmospheric Chemistry Physics* 23, 10489–10516, https://doi.org/10.5194/acp-23-10489-2023

Li, G, J Wieder, JT Pasquier, J Henneberger, and ZA Kanji. "Predicting atmospheric background number concentration of ice-nucleating particles in the Arctic." *Atmospheric Chemistry Physics* 22, 14441–14454, https://doi.org/10.5194/acp-22-14441-2022

Möhler, O, M Adams, L Lacher, F Vogel, J Nadolny, R Ullrich, C Boffo, T Pfeuffer, A Hobl, M Weiß, HSK Vepuri, N Hiranuma, and BJ Murray. 2021. "The Portable Ice Nucleation Experiment (PINE): a new online instrument for laboratory studies and automated long-term field observations of ice-nucleating particles." *Atmospheric Measurement Techniques* 14, 1143–1166, https://doi.org/10.5194/amt-14-1143-2021

Niemand, M, O Mohler, B Vogel, H Vogel, C Hoose, P Connolly, H Klein, H Bingemer, P DeMott, J Skrotzki, and T Leisner. 2012. "A Particle-Surface-Area-Based Parameterization of Immersion Freezing on Desert Dust Particles." *Journal of Atmospheric Sciences* 69, 3077–3092, https://doi.org/10.1175/jas-d-11-0249.1

Rinaldi, M, N Hiranuma, G Santachiara, M Mazzola, K Mansour, M Paglione, CA Rodriguez, R Traversi, S Becagli, D Cappelletti, and F Belosi. 2021. "Ice-nucleating particle concentration measurements from Ny-Ålesund during the Arctic spring–summer in 2018." *Atmospheric Chemistry Physics* 21, 14725–14748, https://doi.org/10.5194/acp-21-14725-2021

Shupe, MD. 2011. "Clouds at Arctic Atmospheric Observatories. Part II: Thermodynamic Phase Characteristics." *Journal of Applied Meteorology and Climatology* 50, 645–661, https://doi.org/10.1175/2010jamc2468.1

Sorribas, M, BA de la Morena, B Wehner, JF López, N Prats, S Mogo, A Wiedensohler, and VE Cachorro. 2011. "On the sub-micron aerosol size distribution in a coastal-rural site at El Arenosillo Station (SW – Spain)." *Atmospheric Chemistry Physics* 11, 11185–11206, https://doi.org/10.5194/acp-11-11185-2011

Vali, G.1971. "Quantitative Evaluation of Experimental Results an the Heterogeneous Freezing Nucleation of Supercooled Liquids." *Journal of Atmospheric Sciences* 28, 402–409, https://doi.org/10.1175/1520-0469(1971)028<0402:QEOERA>2.0.CO;2

Wilbourn, EK, L Lacher, C Guerrero, HSK Vepuri, K Höhler, J Nadolny, AD Pantoya, O Möhler, and N Hiranuma. 2024. "Measurement report: A comparison of ground-level ice-nucleating-particle abundance and aerosol properties during autumn at contrasting marine and terrestrial locations." *Atmospheric Chemistry Physics* 24, 5433–5456, https://doi.org/10.5194/acp-24-5433-2024

Table S1. Summary of the ambient aerosol particle filter sampling conditions at NOAA's Barrow Atmospheric Baseline Observatory.

Sample ID	Start Time (UTC)	End Time (UTC)	Flow Rate (LPM)*	Air Volume, V_{air} (L STP)	Suspension Water Volume, V_l (mL)	Aerosol Surface Area Conc., S_{aer} (m^2 L^{-1})**	Air Temperature (°C)	Relative Humidity (%)	Wind Speed (m s^{-1})	Wind Direction (°)	Cumulative Rainfall (inch)
NSA1	10/22/21 19:00	10/25/21 21:04	6.1	13576.4	2.8	1.2E-09 ± 2.0E-10	-2.7 ± 0.4	92.7 ± 2.3	4.9 ± 1.7	139.6 ± 141.3	0.05
NSA2	10/25/21 21:21	10/29/21 18:19	3.7	10291.4	2.1	5.5E-10 ± 1.5E-10	-8.0 ± 4.8	92.2 ± 3.6	3.8 ± 1.5	137.6 ± 37.3	0.19
NSA3	10/29/21 18:41	11/1/21 21:53	3.0	6745.4	1.4	1.7E-09 ± 1.3E-09	-7.9 ± 4.5	90.3 ± 4.5	5.8 ± 3.4	154.2 ± 48.6	0.03
NSA4	11/1/21 22:12	11/5/21 17:05	3.5	9665.4	2.0	5.2E-09 ± 3.9E-09	-8.0 ± 4.0	89.2 ± 4.6	7.5 ± 2.6	124.5 ± 107.3	0.00
NSA5	11/5/21 17:23	11/8/21 22:41	3.6	8394.8	1.8	6.2E-09 ± 4.3E-09	-7.1 ± 2.8	87.6 ± 5.6	6.8 ± 3.2	111.0 ± 75.8	0.00
NSA6	11/8/21 23:00	11/12/21 19:38	3.6	10004.4	2.1	1.0E-09 ± 4.8E-10	-7.5 ± 0.8	85.7 ± 5.5	7.2 ± 1.4	116.8 ± 113.8	0.12
NSA7	11/12/21 19:55	11/15/21 21:02	3.9	8455.9	1.8	3.3E-10 ± 0.0E+00	-10.6 ± 2.4	81.2 ± 3.5	5.4 ± 1.6	265.8 ± 78.4	0.08
NSA8	11/15/21 21:13	11/22/21 21:06	2.0	9921.9	2.1	2.3E-09 ± 2.7E-09	-16.4 ± 3.5	83.2 ± 2.3	5.6 ± 2.1	141.2 ± 149.5	0.05
NSA9	11/22/21 21:18	11/26/21 23:32	3.9	11493.3	2.4	1.6E-09 ± 4.4E-10	-20.0 ± 1.9	82.5 ± 1.5	5.3 ± 2.1	102.7 ± 89.1	0.01
NSA10	11/26/21 23:39	11/29/21 21:23	4.0	8263.4	1.7	1.6E-09 ± 3.7E-10	-24.9 ± 1.6	79.2 ± 1.5	4.1 ± 1.5	66.6 ± 39.9	0.01
NSA11	11/29/21 21:31	12/3/21 21:11	1.7	5008.2	1.0	1.2E-09 ± 3.0E-10	-26.9 ± 1.4	77.7 ± 1.7	5.5 ± 2.7	71.3 ± 47.4	0.01
NSA12	12/3/21 21:18	12/6/21 23:41	4.1	9149.2	1.9	5.7E-09 ± 4.0E-10	-12.1 ± 5.4	83.9 ± 2.8	8.6 ± 1.4	161.1 ± 27.1	0.04
NSA15	12/13/21 21:32	12/18/21 0:32	4.0	12013.7	2.5	4.9E-09 ± 2.6E-09	-26.2 ± 2.3	77.9 ± 1.5	6.5 ± 4.5	127.5 ± 82.4	0.22
NSA16	12/18/21 0:36	12/20/21 21:06	3.9	8035.0	1.7	4.8E-09 ± 1.5E-09	-17.7 ± 6.7	84.8 ± 5.9	9.6 ± 3.6	115.2 ± 60.2	0.51
NSA17	12/20/21 21:11	12/31/21 23:00	3.7	29585.4	6.2	3.1E-09 ± 1.1E-09	-24.8 ± 3.9	79.0 ± 2.8	6.1 ± 2.9	209.9 ± 117.2	0.29
NSA57	6/6/22 23:49	6/10/22 19:10	5.8	15853.8	3.3	5.1E-10 ± 1.6E-10	-2.9 ± 1.6	93.1 ± 2.9	5.1 ± 1.7	179.7 ± 129.1	0.01
NSA58	6/10/22 19:15	6/13/22 19:58	5.7	12532.7	2.6	2.1E-10 ± 1.0E-10	-2.1 ± 1.2	95.2 ± 2.6	3.8 ± 1.8	94.8 ± 114.7	0.02
NSA59	6/13/22 20:10	6/17/22 23:32	5.6	16827.7	3.5	4.7E-10 ± 4.7E-10	1.0 ± 1.6	94.5 ± 2.4	4.3 ± 1.5	127.0 ± 86.0	0.01
NSA60	6/17/22 23:39	6/24/22 16:45	5.6	27016.5	5.6	8.5E-10 ± 6.6E-10	4.3 ± 3.6	91.9 ± 8.0	4.0 ± 1.3	178.7 ± 66.3	0.15
NSA61	6/24/22 16:49	6/27/22 19:07	5.8	12861.3	2.7	1.2E-09 ± 8.2E-10	8.4 ± 3.8	N/A ± N/A	3.4 ± 1.3	133.8 ± 46.2	0.07
NSA62	6/27/22 19:14	7/1/22 19:34	5.9	16949.9	3.5	1.6E-09 ± 7.4E-10	5.0 ± 3.4	94.8 ± 3.7	4.4 ± 1.2	127.1 ± 79.4	0.21
NSA80	8/29/22 18:53	9/5/22 19:51	5.7	29045.4	6.1	8.7E-10 ± 7.3E-10	2.9 ± 0.5	N/A ± N/A	4.8 ± 2.2	80.0 ± 34.4	0.03
NSA82	9/5/22 20:16	9/9/22 21:30	5.8	17035.3	3.6	1.3E-09 ± 1.6E-09	2.2 ± 1.3	N/A ± N/A	6.4 ± 1.9	92.1 ± 17.2	0.00
NSA83	9/9/22 21:34	9/12/22 21:39	5.8	29045.4	6.1	1.2E-09 ± 5.7E-10	1.5 ± 0.4	N/A ± N/A	8.4 ± 0.8	85.9 ± 7.6	0.00
NSA84	9/12/22 21:47	9/16/22 21:10	5.7	16296.2	3.4	4.0E-09 ± 1.2E-09	1.4 ± 0.4	N/A ± N/A	11.2 ± 0.8	92.6 ± 9.4	0.06
NSA85	9/16/22 21:15	9/19/22 18:07	5.8	11972.5	2.5	2.2E-09 ± 1.1E-09	1.5 ± 1.5	N/A ± N/A	9.2 ± 3.7	114.5 ± 30.5	0.00
NSA86	9/19/22 18:15	9/23/22 17:46	5.7	16419.3	3.4	8.2E-10 ± 3.2E-10	2.3 ± 2.0	N/A ± N/A	4.3 ± 1.5	127.4 ± 47.4	0.05
NSA87	9/23/22 17:50	9/26/22 17:34	5.7	12320.2	2.6	1.8E-09 ± 7.8E-10	-0.6 ± 1.0	N/A ± N/A	7.2 ± 1.9	74.2 ± 18.1	0.04
NSA88	9/26/22 17:41	9/30/22 17:21	5.7	16301.6	3.4	1.8E-09 ± 1.1E-09	-1.2 ± 0.6	N/A ± N/A	7.0 ± 1.5	99.6 ± 71.2	0.07
NSA89	9/30/22 17:26	10/3/22 20:17	5.8	12934.1	2.7	6.6E-10 ± 3.0E-10	-0.3 ± 3.3	N/A ± N/A	6.6 ± 3.2	168.1 ± 33.1	0.10
NSA91	10/3/22 20:40	10/7/22 17:59	5.7	15999.1	3.3	3.2E-10 ± 4.1E-11	-2.5 ± 1.0	N/A ± N/A	5.8 ± 1.2	110.9 ± 80.9	0.02
NSA94	10/14/22 18:20	10/17/22 18:01	5.7	12311.6	2.6	4.8E-09 ± 3.0E-09	-4.1 ± 3.5	N/A ± N/A	6.9 ± 2.6	136.2 ± 64.6	0.01
NSA95	10/17/22 18:08	10/21/22 17:39	5.7	16347.7	3.4	2.1E-09 ± 9.7E-10	-3.1 ± 1.0	N/A ± N/A	6.7 ± 2.8	107.2 ± 43.0	0.05
NSA96	10/21/22 17:49	10/24/22 18:38	5.8	12713.8	2.7	1.1E-09 ± 4.4E-10	-4.1 ± 1.5	N/A ± N/A	10.1 ± 0.8	117.3 ± 6.3	0.01
NSA97	10/24/22 18:41	10/28/22 18:05	5.8	16499.4	3.4	1.1E-09 ± 3.9E-10	-6.1 ± 1.0	N/A ± N/A	8.1 ± 2.3	96.5 ± 22.1	0.28
NSA98	10/28/22 18:14	10/31/22 21:43	5.8	13020.9	2.7	1.4E-09 ± 6.4E-10	-7.3 ± 2.8	N/A ± N/A	7.7 ± 2.6	99.5 ± 17.3	0.16
NSA99	10/31/22 22:12	11/4/22 16:54	5.8	15849.8	3.3	9.0E-10 ± 4.1E-10	-11.8 ± 3.8	N/A ± N/A	3.6 ± 1.6	142.8 ± 50.6	0.07

* The averaged relative standard deviation of air flow rate during individual sampling (beginning - end) is <6%. A mass flow controller or a critical orifice was used to ensure a constant flow throughout each sampling activity. An airflow rate was measured with a flowmeter (TSI Inc., model 4140). ** We estimated the aerosol surface area concentration (S_{aer}) at the volume standard temperature and pressure (273 K and 1013.25 hPa, respectively) using the NOAA's aerosol scattering coefficients measured by an integrating nephelometer (Model 3563, TSI Inc.). The application of the nephelometer data to calculate the aerosol surface areas is described in Wilbourn et al. (2024) and Pantoya et al. (submitted). An effective aerosol scattering efficiency, Q, of 2.37 from El Arenosillo, Spain, is considered a representative Q for clean marine conditions and is used in this study (Sorribas et al., 2019).

www.arm.gov

U.S. DEPARTMENT OF
ENERGY

Office of Science